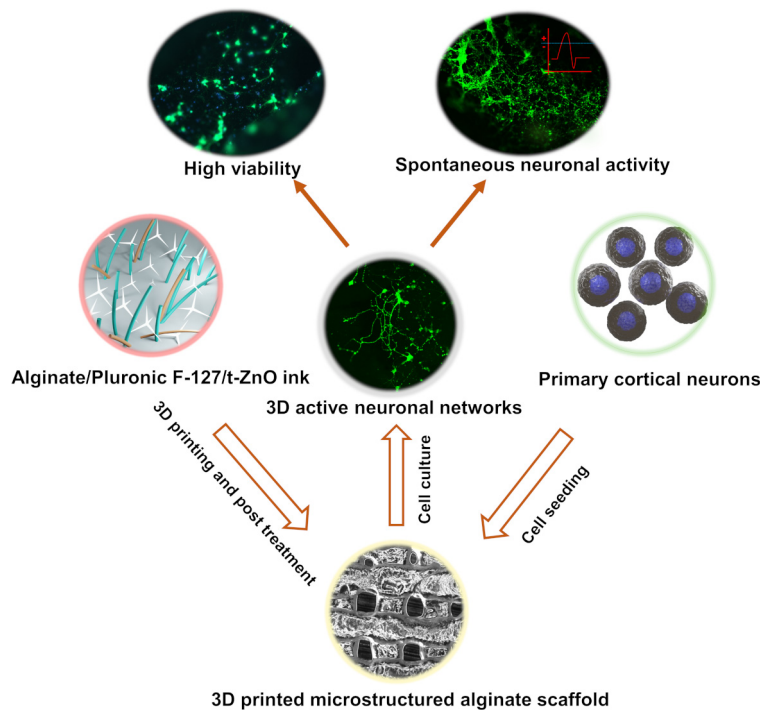


Resource Article

3D-printed microstructured alginate scaffolds for neural tissue engineering



Tetrapod-shaped ZnO (t-ZnO) microparticles create interconnected channels and textured surfaces in 3D-printed microstructured alginate (M-Alg) scaffolds. Primary mouse cortical neurons cultured on the M-Alg scaffolds demonstrate enhanced adhesion and maturation, with extensive 3D neural projections forming, indicating the potential of this scaffold design for advanced neural tissue engineering applications.

Jianfeng Li, Benjamin Hietel, Michael G.K. Brunk, Armin Reimers, Christian Willems, Thomas Groth, Holger Cynis, Rainer Adelung, SchuttFabian Schütt, Wesley D. Sacher, Joyce K.S. Poon

jianfeli@mpi-halle.mpg.de (J. Li).

Highlights

Tetrapod-shaped ZnO (t-ZnO) microparticles create interconnected channels and textured surfaces in 3D-printed microstructured alginate (M-Alg) scaffolds.


Primary mouse cortical neurons cultured on the M-Alg scaffolds demonstrate enhanced adhesion and maturation, with formation of extensive 3D neural projections, indicating the potential of this scaffold design for advanced neural tissue engineering applications.

Trends in Biotechnology, Month 2024,
Vol. xx, No. xx

<https://doi.org/10.1016/j.tibtech.2024.10.013>

Resource Article

3D-printed microstructured alginate scaffolds for neural tissue engineering

Jianfeng Li ^{1,2,*}, Benjamin Hietel³, Michael G.K. Brunk^{1,2}, Armin Reimers⁴, Christian Willems⁵, Thomas Groth⁵, Holger Cynis^{3,6}, Rainer Adelung⁴, Fabian Schütt⁴, Wesley D. Sacher^{1,2}, and Joyce K.S. Poon^{1,2,7}

Alginate (Alg) is a versatile biopolymer for scaffold engineering and a bioink component widely used for direct cell printing. However, due to a lack of intrinsic cell-binding sites, Alg must be functionalized for cellular adhesion when used as a scaffold. Moreover, direct cell-laden ink 3D printing requires tedious disinfection procedures and cell viability is compromised by shear stress. Here, we demonstrate proof-of-concept, bioactive additive-free, microstructured Alg (M-Alg) scaffolds for neuron culture. The M-Alg scaffold was formed by introducing tetrapod-shaped ZnO (t-ZnO) microparticles into the ink as structural templates for interconnected channels and textured surfaces in the 3D-printed Alg scaffold, which were subsequently removed. Neurons exhibited significantly improved adhesion and growth on these M-Alg scaffolds compared with pristine Alg (P-Alg) scaffolds, with extensive neurite outgrowth and spontaneous neural activity, indicating the maturation of neuronal networks. These transparent, porous, additive-free Alg-based scaffolds with neuron affinity are promising for neuroregenerative and organoid-related research.

Introduction

In vitro 3D cellular models are a method for replicating the physiological microenvironments of *in vivo* tissues, serving as useful supplements to animal models and *ex vivo* tissues. These 3D models complement pathophysiological models and elucidate the mechanisms that govern cellular behaviors for advancing our understanding of various diseases [1]. 3D neural models serve as an analog of their *in vivo* counterpart for investigating therapies for neurological disorders and studying the mechanisms of neural computation. Among the various fabrication methods for 3D cell models, 3D bioprinting stands out for its ability to fabricate models with precise anatomical features and to incorporate multiple bioactive components in a programmable fashion [2,3]. Although extrusion-based 3D bioprinting, which utilizes bioink to encapsulate living cells, is popular, the effective disinfection of cell-laden ink and mitigation of shear stress on cell viability during the printing process are critical challenges [4,5]. An alternative approach is to initially print a **scaffold** (see [Glossary](#)), followed by sterilization and cell seeding [6]. Here, the scaffold should have interconnected pores to facilitate nutrient and waste transport, **vascularization**, and cell migration during the tissue regeneration process [7]. 3D printing can be used to fabricate porous scaffolds by offering greater control over the scaffold architecture [8] and components [9,10] compared with other fabrication strategies, such as salt leaching, microsphere sintering, and electrospinning [11]. However, in 3D-printed scaffolds, cells are usually confined to the surface, leaving the internal volume devoid of cells due to the barrier properties of the printed material. This may result in diminished cell-loading capacity and compromised intercellular communication.

Technology readiness

In vitro 3D neural models mimic *in vivo* neural systems, providing a platform for studying therapies and neural computation. Alginate (Alg) is a scaffold widely used in tissue engineering, particularly with the rise of 3D-bioprinting technologies. However, Alg lacks cell-anchoring points and often requires bioactive additives for effective cell seeding after printing. Our study introduced bioactive additive-free, microstructured Alg (M-Alg) scaffolds for 3D neuron culture. Neurons displayed significantly improved adhesion and growth on M-Alg scaffolds compared with pristine Alg (P-Alg) scaffolds, along with enhanced neurite outgrowth and spontaneous neural activity, indicating neuronal network maturation. Further studies are required to explore the potential of this system for high-throughput drug testing, transplantation in animal models, and neuronal computation in artificial systems. Insights from these tests will inform scaffold design, with broader applications across various fields in the future.

¹Max Planck Institute of Microstructure Physics, Weinberg 2, Halle, 06120, Germany

²Max Planck-University of Toronto Centre for Neural Science and Technology, Toronto, Canada

³Department of Drug Design and Target Validation, Fraunhofer Institute for Cell Therapy and Immunology, Weinbergweg 22, 06120, Halle, Germany

⁴Functional Nanomaterials, Department of Materials Science, Kiel University, Kaiserstraße 2, 24143 Kiel, Germany

⁵Department of Biomedical Materials, Institute of Pharmacy, Martin Luther University Halle-Wittenberg, 06120, Halle, Germany

Alg, which has a similar linear polysaccharide structure to naturally occurring hyaluronic acid in the brain extracellular matrix, is a well-established biopolymer derived from brown algae and has found numerous applications since its discovery over a century ago [12,13]. In particular, Alg solutions can form gels through ionic crosslinking in a biocompatible manner [13], eliminating the need for additional chemical modifications [14] or the use of toxic agents, such as carbodiimide or other chemical crosslinkers [15]. Thus, Alg is an ideal material for 3D cell culture, serving as a cell niche either through direct cell encapsulation within the Alg gel or by seeding cells on the scaffold after fabrication [16,17]. Direct cell-seeding efficiency on the Alg scaffold is only 18%, which is much lower than the 95–115% seeding efficiency using cell-laden Alg solutions [18]. The reason for this is the lack of cell-anchoring ligands in Alg, such that cell seeding on Alg scaffolds is less effective compared with encapsulating cells directly within the Alg structure after gelation. To improve the cell-seeding efficiency on Alg scaffolds, the scaffold surfaces can be modified with bioactive components [e.g., arginine-glycine-aspartic acid (RGD) and collagen] or functional coatings to promote cell attachment and growth [6,13,19], but this may not always be compatible with the chemical or physiological tests for which the scaffold is intended.

Regarding the encapsulation of cells in Alg, a drawback, especially at high Alg concentrations, is that the cells suffer from limited access to nutrition and oxygen, a slow waste removal rate, and high stress due to the strong bonding of Alg polymer chains [20]. This results in low cell viability, particularly after long-term culture, although artificial channels created within the bulky Alg structure could mitigate the issue [20]. The channels may be 3D printed and Alg has been extensively applied in 3D bioprinting since it is easy to print and retains the printed structure in the presence of calcium ions [21,22]. However, 3D bioprinting of cell-laden Alg ink applies shear stress to the cells and increases the risk of contamination, reducing the viability of the printed cells [23].

In this study, we present a technique for creating transparent, additive-free, M-Alg scaffolds with varying diameter channels and textured surfaces that have high cellular affinity (Figure 1). Using **tetrapod-shaped ZnO (t-ZnO)** microparticles as templates, which are later removed, we produced scaffolds that encouraged neuron adhesion, proliferation, and circuit formation without the need for pretreatments or bioink modifications. t-ZnO microparticles were selected as the template for their four-armed shape with varying dimensions and for their ease of removal

⁶Junior Research Group, Immunomodulation in Pathophysiological Processes, Faculty of Medicine, Martin Luther University Halle-Wittenberg, 06120, Halle, Germany
⁷Department of Electrical and Computer Engineering, University of Toronto, 10 King's College Road, Toronto, Ontario, Canada

*Correspondence: jianfeli@mpi-halle.mpg.de (J. Li).

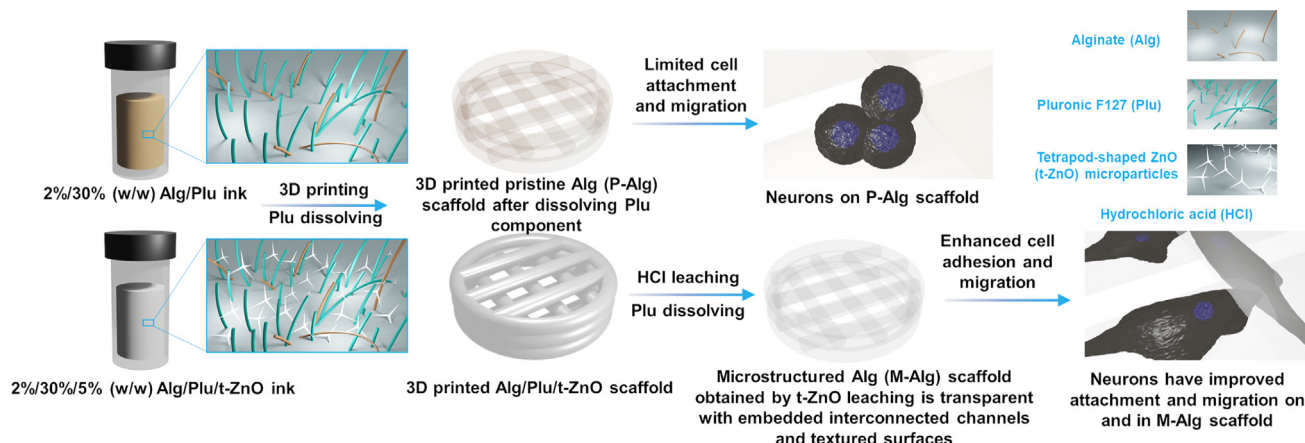


Figure 1. Schematic depiction of the 3D printing process contrasting pristine alginate (P-Alg) scaffolds and microstructured Alg (M-Alg) scaffolds with interconnected channels and textured surfaces. Neurons exhibit improved adhesion and proliferation on M-Alg scaffolds, while showing limited adhesion on P-Alg scaffolds. Abbreviations: HCl, hydrochloric acid; Plu, pluronic F127; t-ZnO, tetrapod-shaped ZnO.

using evaporating acid (hydrochloric acid: HCl), which are features essential for forming multi-sized interconnected channels in the scaffold. Interconnected channels in scaffolds offer pathways for vascularization, nutrient transport, waste disposal, and cell migration. Multi-sized channels are particularly beneficial for tissue regeneration [6,24]. Bioinert Pluronic F-127 (Plu) was used to modify the rheological properties of the printed ink and it was fully removed during the fabrication process [22]. Alg scaffolds with uniformly sized channels have previously been shown to promote blood vessel growth without inflammation or abnormalities after 3 weeks of implantation [25] and facilitate controlled delivery of therapeutics [26]. Compared with pristine Alg (P-Alg) scaffolds, in a series of proof-of-concept experiments, M-Alg scaffolds with interconnected channels were found to be more conducive to the adhesion, proliferation, migration, and establishment of active circuits of primary mouse neurons seeded on the structure. We hypothesize that the internal channels and textured surfaces [27] enhanced the efficacy of M-Alg scaffolds in peripheral nerve generation based on the previously reported results [28]. This approach of forming porous Alg scaffolds reduces variability in cellular responses, offering a potential alternative to Matrigel as a biomaterial.

Results and discussion

3D-printed Alg-based scaffold with open interconnected channels and textured surfaces

Alg is widely recognized for its versatility in biomedical applications, but its use in tissue engineering has been limited by the absence of bioactive ligands. Enhancing the cellular affinity of Alg without functionalization could expand its use by reducing complications from foreign materials. We used t-ZnO microparticles as templates to modify the morphology and internal structure of 3D-printed Alg scaffolds. The t-ZnO microparticles, characterized by four arms, naturally assemble into interlinked networks in close proximity (Figure 2A–C). During the ink preparation process, t-ZnO microparticles settled at the bottom of the ink to form interlinked networks after centrifugation and were then used directly for 3D scaffold printing (Figure S1 in the supplemental information online). Remarkably, these microparticles can be easily eliminated using a hydrophilic volatile acid (such as HCl), ensuring the absence of toxic residues post fabrication, which is preferred over conventional particulate leaching using organic solvents, such as dimethylformamide [29]. The acid treatment does not affect the morphology and surface of 3D-printed Alg scaffolds because the Alg structure is chemically inert to HCl [30].

The 3D-printed P-Alg scaffold exhibited optical transparency (Figure 2D). However, upon integrating t-ZnO microparticles, the structure assumed a white hue, although the print quality was preserved (Figure 2E,H and Figure S2A in the supplemental information online). Our previous study indicated that inks containing t-ZnO microparticles exhibit favorable rheological attributes at room temperature (RT) for 3D printing [22]. Leaching in HCl reinstates the transparency of the structure, along with a textured morphology, while preserving mechanical integrity (Figures 2F,G,I and Figure S2B and Video S1 in the supplemental information online). Incorporating t-ZnO microparticles into Alg-based ink yields a roughened printed framework, which persists as a network within the hydrogel matrix (Figure 2J–O). The porosity introduced by the incorporation of t-ZnO microparticles in the microstructured scaffolds was estimated through calculation to be 1.1%. Compared with 3D Alg scaffolds fabricated by freeze gelation [31], freeze drying [32], and 3D printing [6], our proposed fabrication strategy enables more control over the overall shape, transparency, and introduction of pores/channels with a range of size distributions.

Neuron adhesion, viability, and proliferation on 3D scaffolds

Cell adhesion and viability within supportive structures are crucial to successful engineering of tissues, affecting cellular migration, proliferation, and differentiation [33]. Primary cortical neurons adhered initially to both P-Alg and M-Alg scaffolds; however, M-Alg scaffolds demonstrated significantly

Glossary

Alginate (Alg): biocompatible polysaccharide that originates from brown algae. Its aqueous solution is viscous and can gel efficiently with divalent and multivalent cations.

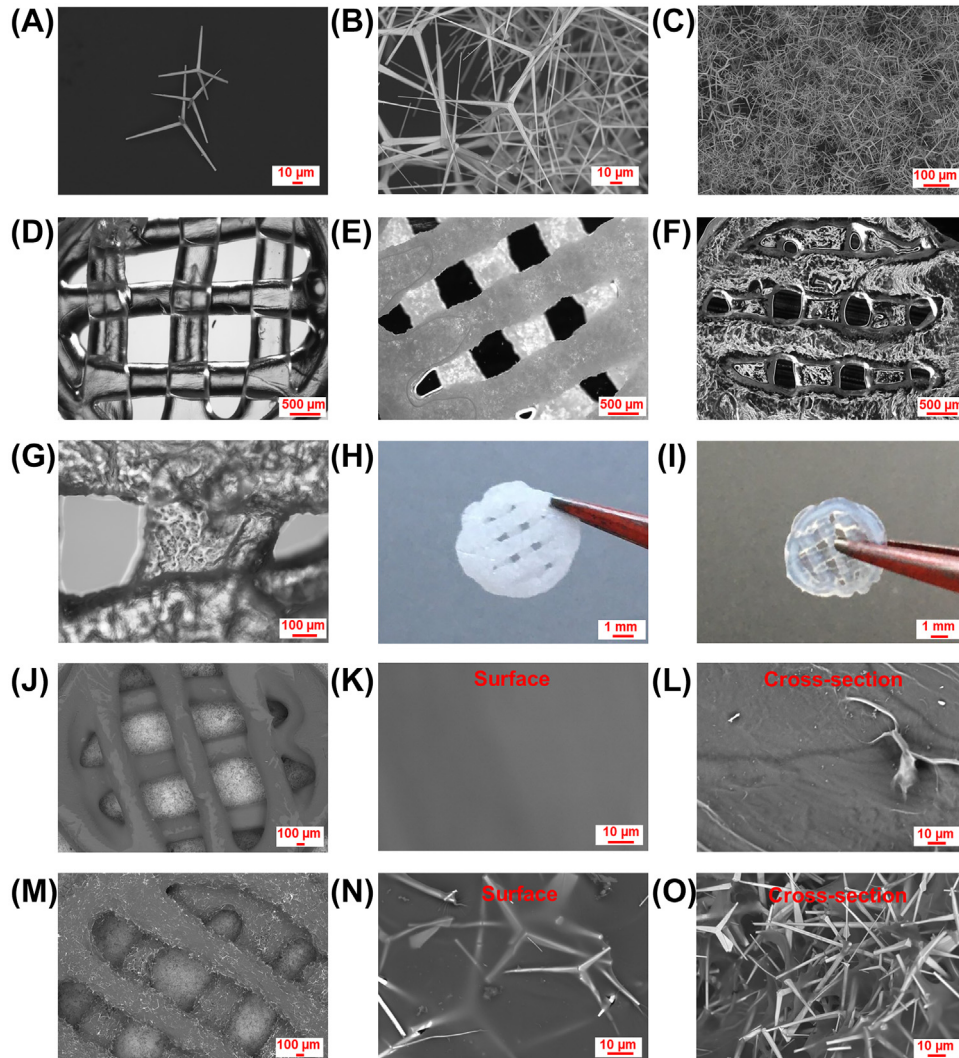
Neural network: neurites extending from neurons connect with each other through synapses to form a neural network. Neurons can interact efficiently within the same neural network, providing a new paradigm for computer architecture design.

Scaffold: 3D constructions that support cell or tissue growth in tissue engineering, usually presenting with physicochemical cues. The scaffold should be porous to allow the free passage of nutrients, oxygen, and waste.

Spontaneous neural activity: neurons fire to communicate with each other within neural networks in the absence of sensory input.

Tetrapod-shaped ZnO (t-ZnO): form of ZnO crystal structure with four hexagonal arms and one core. t-ZnO can react with HCl and the resulting $ZnCl_2$ is highly soluble in water.

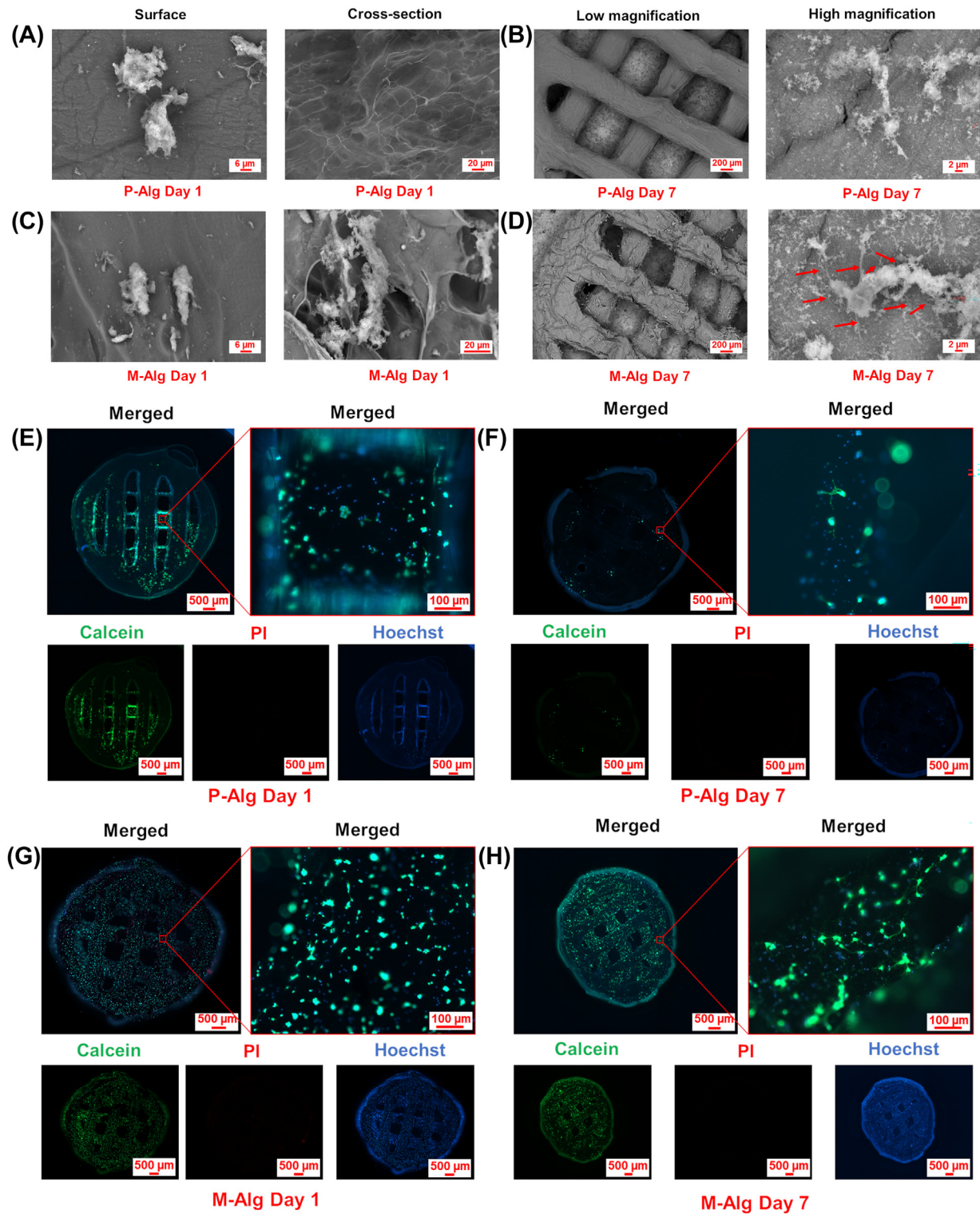
Vascularization: formation of new blood vessels within a tissue. It is critical for the survival of thick tissues, because oxygen diffusion is only effective when the tissue is avascular and thinner than 200 μm . Vascularized tissues can receive enhanced oxygen and nutrient delivery.



Trends in Biotechnology

Figure 2. Morphology of 3D-printed pristine alginate (P-Alg) scaffolds and microstructured Alg (M-Alg) scaffolds. (A–C) Scanning electron microscopy (SEM) images of different concentrations of tetrapod-shaped ZnO (t-ZnO) microparticles. Optical microscope images of a 3D-printed (D) P-Alg scaffold, (E) 2%/30%/5% (w/w) Alg/Plu/t-ZnO scaffold, and (F,G) M-Alg scaffold at various magnifications. Photographs of 3D-printed (H) 2%/30%/5% (w/w) Alg/Plu/t-ZnO scaffold and (I) M-Alg scaffold. SEM images of an overview of (J) a 3D-printed P-Alg scaffold with magnified (K) surface and (L) cross-sectional morphology. SEM images of a 3D-printed (M) 2%/30%/5% (w/w) Alg/Plu/t-ZnO scaffold with magnified (N) surface and (O) cross-sectional morphology.

better and more uniformly distributed cellular adhesion with neurons that exhibited a spread morphology (Figure 3A,C,E,G). Neurons seeded onto the M-Alg scaffolds could infiltrate the open channels, substantially increasing the filling of the scaffold architecture (Figure 3C). Despite the initial cellular adhesion on both scaffold types, adhesion on P-Alg scaffolds was only temporary, with a round morphology of cells followed by a markedly decrease in cellular presence by Day 7 (Figure 3B,D,F,H). By contrast, neurons formed durable connections on M-Alg scaffolds, extending neurite anchors throughout (Figure 3D) and maintained high-density populations with complex **neural networks** by Day 7 (Figure 3H). After a 7-day culture period, the P-Alg scaffolds appeared smooth, whereas M-Alg scaffolds showed a rough texture with visible t-ZnO shapes, due to internally



Trends in Biotechnology

(See figure legend at the bottom of the next page.)

connected channels (Figure S3A–D in the supplemental information online). These results show the benefit of textured, rough scaffolds based on M-Alg scaffolds, with internal channels promoting neuron adhesion and growth in contrast to the smooth and hydrophilic characters of P-Alg scaffolds, which obviously did not support durable attachment of cells. Our results are consistent with previous publications that show that pristine Alg scaffolds have limited ability to support cell growth [6,18,34]. In contrast to conventional methods of introducing external bioactive moieties or molecules, such as conjugating functional groups, including Tyramine [34] or RGD [35], or mixing with biomaterials (e.g., collagen [13] or graphene oxide [21]) to increase the bioactivity of 3D Alg structures, our approach physically modifies Alg to create topographical cues that serve as cell anchoring points, promoting cell adhesion and growth. Without functionalization of the material or scaffold, cells encapsulated in Alg form only aggregates and not an interconnected cellular network with a spread cell morphology [13,18]. Thus, Alg scaffolds with only structural modifications that show improved cell support will provide more opportunities for relevant fields.

The influence of P-Alg and M-Alg scaffolds on neuronal proliferation and metabolic activity was tested with the PrestoBlue assay. Neurons exhibited proliferation and metabolic activity on both scaffolds, with the number of neurons and metabolic activity on M-Alg scaffolds significantly higher than on the P-Alg scaffolds groups (Figure 4). The significantly higher neuron numbers and metabolic activity observed on M-Alg Day7 may be attributed to the increased surface area conducive to neuron growth and enhanced nutrition/oxygen transport facilitated by the channels embedded within the scaffold. Additionally, nongelling ions or molecules in the culture medium can distort the crosslinked calcium Alg networks, leading to reduced mechanical strength, structure swelling, and, eventually, complete structure dissolution [6,36]. M-Alg scaffolds exposed a higher surface area to the nongelling agents compared with P-Alg scaffolds, resulting in a softer nature of the porous M-Alg scaffolds, which might contribute to enhanced neuron growth and metabolic activity [37]. Two-way ANOVA analyses revealed the significant influence of both scaffold type [$F(1,36) = 29.8, P < 0.01$] and neuron culture time [$F(1,36) = 147.2, P < 0.01$] on neuron proliferation and metabolic activity. Thus, M-Alg scaffolds show promise as improved substrates supporting neuronal cell proliferation and metabolic activity.

Neuron maturation evaluation

Neuronal cells develop morphological, electrophysiological, and molecular features as they mature [38]. To evaluate neuron maturation with the M-Alg scaffold, 3D neuronal cultures were stained with the calcium-sensitive dye Calbryte 520 and markers of β -tubulin III and synaptophysin to differentiate neuronal phenotypes. Significant neuron outgrowth, spanning several hundred micrometers, was observed in the M-Alg scaffolds on Day 8 (Figure 5A,B) after staining with Calbryte 520, which also indicated functional activity given the presence of intracellular free calcium [39]. With an additional week of culture, an even more complex assembly of neuronal networks emerged, accompanied by widespread distribution of dendritic spines throughout the network (Figure 5C,D). This development suggests the potential for increased plasticity in these neuronal networks when cultured in M-Alg scaffolds [40].

Spontaneous neuronal activity was detected in the established neuronal network formed in the modified M-Alg scaffolds by Day 8 (Figure 6 and Video S2 in the supplemental information online). This activity revealed signal transmission among cells, indicating that the complex intercellular connections that had formed were functioning.

Figure 3. Adhesion and survival of primary cortical neurons on pristine alginate (P-Alg) scaffolds and microstructured Alg (M-Alg) scaffolds. Scanning electron microscopy (SEM) images highlighting neurons on the surface and interior of (A) P-Alg and (C) M-Alg scaffolds on Day 1. SEM images showing the scaffold and neuron morphology of (B) P-Alg and (D) M-Alg scaffolds at different magnifications on Day 7, with red arrows indicating neurites. Fluorescence microscope images of cells on P-Alg scaffolds on (E) Day 1 and (F) Day 7, and on M-Alg scaffolds on (G) Day 1 and (H) Day 7. Abbreviation: PI, propidium iodide.

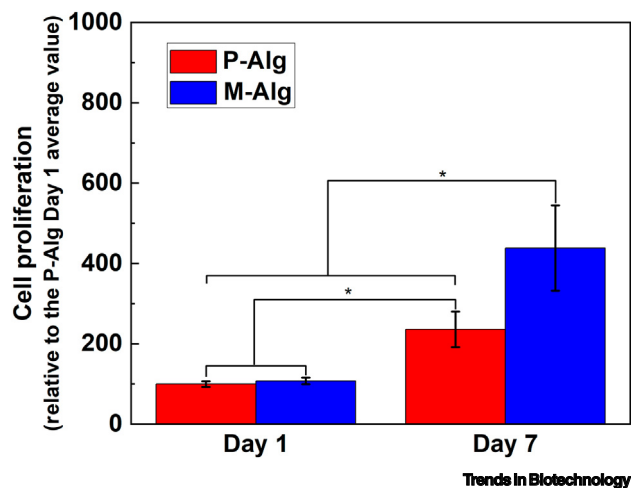


Figure 4. Neuron proliferation and metabolic activity on pristine alginate (P-Alg) scaffolds and microstructured Alg (M-Alg) scaffolds by relative fluorescence intensity increase compared with the P-Alg Day 1 average value. Mean \pm standard deviation (SD), $n = 5$. [Bonferroni post hoc, $P < 0.01$ (M-Alg Day 7 vs. all comparisons; P-Alg Day 7 vs. P-Alg Day 1 and M-Alg Day 1)].

Consistent with the calcium imaging in Figure 5, F-actin staining showed densely branched neuronal networks in the M-Alg scaffolds on Day 5 (Figure 7A and Figure S4 in the supplemental information online). This stands in stark contrast to the notably sparse distribution of neurons

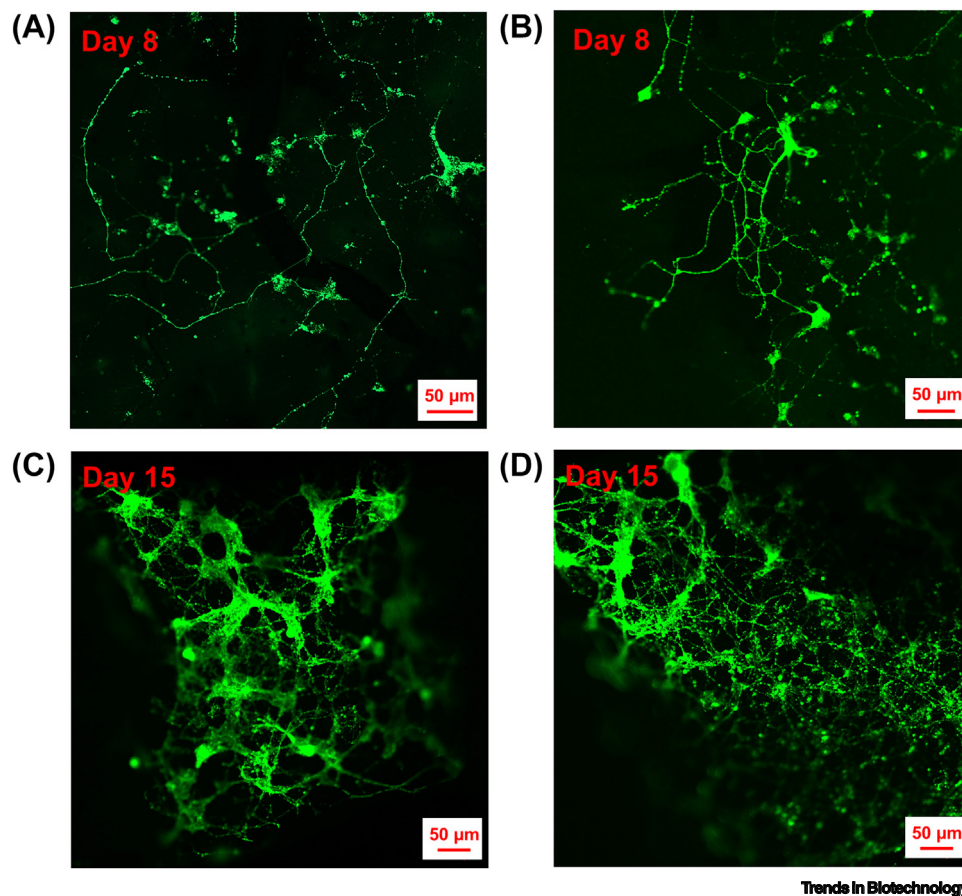


Figure 5. Fluorescence microscopy images showing extended neuronal networks formed in the microstructured alginate (M-Alg) scaffolds on (A,B) Day 8 and (C,D) Day 15. Neuronal network staining was done with Calbryte 520 (green).

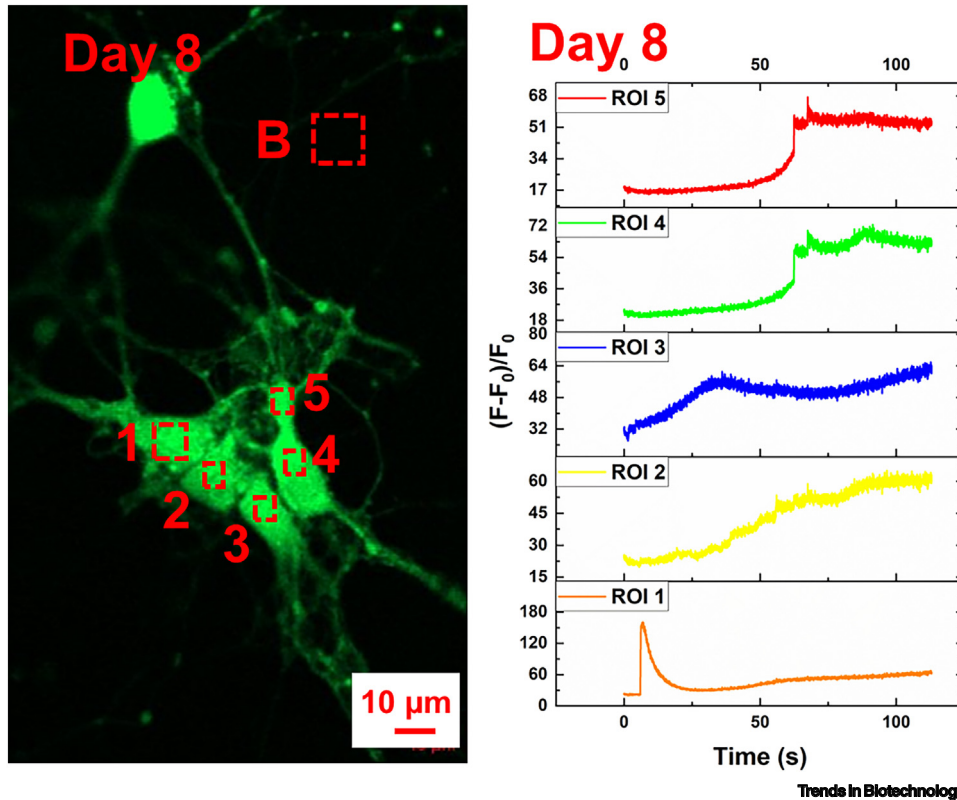


Figure 6. Neuronal networks formed in the microstructured alginate (M-Alg) scaffold show spontaneous activity on Day 8, indicating active intercellular connections formed within the scaffold. Neuronal network stained by Calbryte 520 (green). Numbers 1–5 specify five regions of interest (ROIs) and ‘B’ specifies a background area for subtraction during fluorescence signal processing.

observed on the P-Alg scaffolds on the same day, as well as within both scaffolds on Day 1 (Figure 7B and Figures S5A,B in the supplemental information online). Additionally, staining for the neuronal differentiation marker β -tubulin-III confirmed the development of a complex neuronal network within the M-Alg scaffolds (Figures 7A,B and Figure S4 in the supplemental information online). The presence of synapses, as evidenced by synaptophysin staining, indicates synaptic vesicle formation along the neurites exclusively in the M-Alg scaffolds, showing its ability to support complex neuronal network development and synaptic connectivity, which can be considered as further evidence for the functionality of neuronal networks supported by the porosity and roughness of these types of scaffold (Figures 7A,B and S4). These results complement previously reported 3D functional neuronal networks formed in 3D Alg structures through cell encapsulation with a low Alg ratio (0.1–0.3%) and molecular weight (low viscosity) [41], which are not suitable for 3D printing due to their low viscosity and mechanical strength. Our introduced strategy overcomes the limitations of material properties, offering more opportunities to use a wider range of materials for 3D neural tissue engineering.

Further work is needed to gain a deeper understanding of the phenomena observed at both the macro and micro levels. Future work will include mechanical characterizations of the M-Alg scaffolds, systematically quantifying the effects that the density and size of the microstructured pores/channels have on the regeneration of different tissues, investigations of the transplantation of M-Alg scaffolds *in vivo* for tissue regeneration, longer term robustness, and biodegradation of

the material both *in vitro* and *in vivo*. These current studies pave the way for microstructured Alg scaffolds to serve as novel substrates for *in vitro* neural tissue cultivation and as guiding frameworks for nervous tissue regeneration [42].

Concluding remarks

As a popular material for tissue engineering and bioprinting, Alg has been explored in many studies to expand its potential to tackle longstanding biomedical challenges. However, it lacks cell-anchoring points in its structure and requires special treatment with bioactive additives to be used in supporting cells, which may not always be compatible with intended chemical or physiological tests using the scaffold. Moreover, some additives are costly and sensitive to storage conditions, making real-world applications challenging.

To address this issue, we have described a simple and scalable fabrication strategy to create in-strand, open interconnected channels and textured surfaces in the Alg-based scaffold by combination with t-ZnO microparticles as a templating structure that can be easily dissolved after printing. In proof-of-concept experiments, neurons exhibited robust adhesion and growth on these M-Alg scaffolds (without bioactive additives), with maturation of neuronal networks evidenced by extensive neurite outgrowth and **spontaneous neural activity**, corroborated by the immunohistochemical detection of β -tubulin-III and synaptophysin.

Outstanding questions

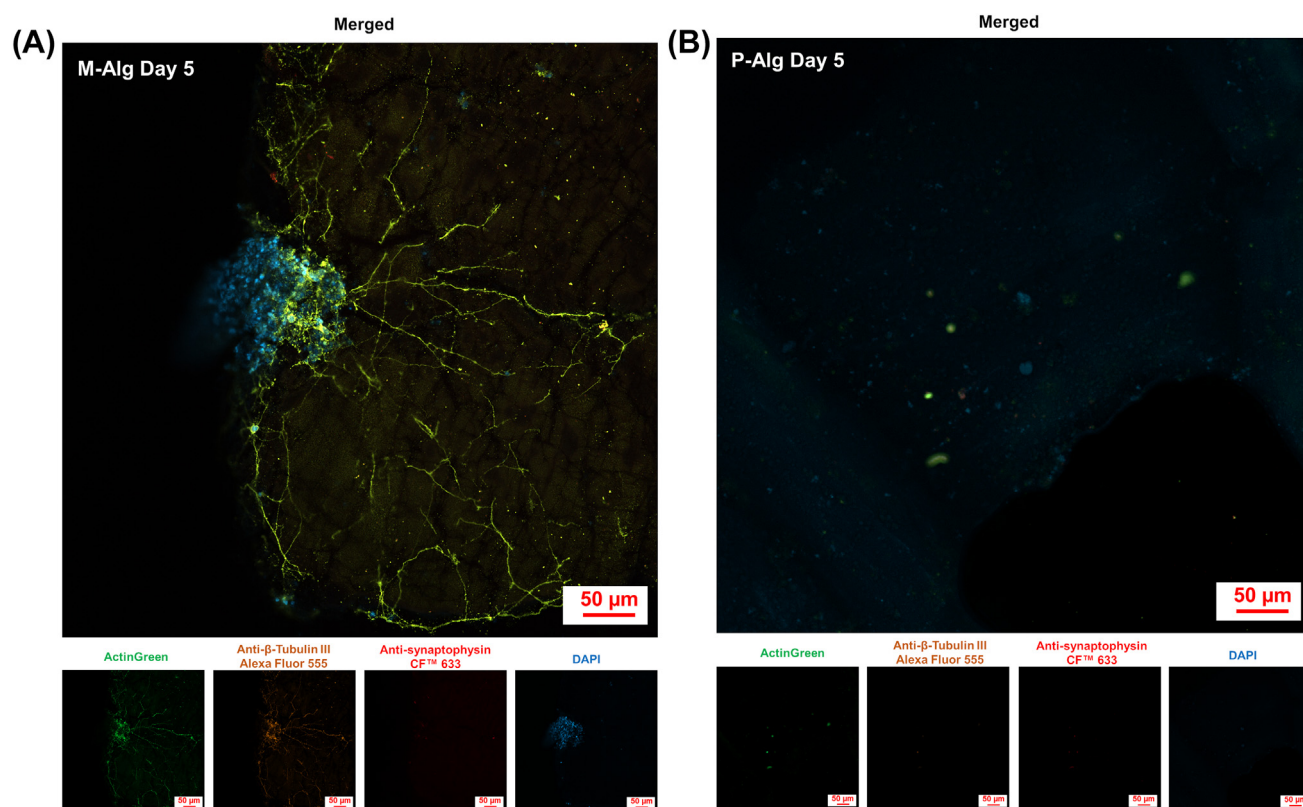
Can the same printing strategies be applied to other bioinert polymers to create suitable 3D scaffolds for neural tissue engineering?

Will there be synergistic effects when applying the method introduced here to bioactive polymers for neural tissue regeneration?

What is the biochemical mechanism behind the influence of the microstructures and interconnected channels on cell physiology?

Can M-Alg scaffolds demonstrate superior performance in other fields of tissue or organoid engineering?

Will the transplantation of M-Alg scaffolds *in vivo* be beneficial for tissue regeneration and disease treatment?



Trends in Biotechnology

Figure 7. Neuronal maturation marker expression in different 3D cultures. Immunofluorescence microscopy of neurons cultured on (A) microstructured alginate (M-Alg) scaffolds and (B) pristine alginate (P-Alg) scaffolds on Day 5. Robust neural network development was observed in M-Alg scaffold compared with sparse neurons on P-Alg scaffold by Day 5. F-actin stained with ActinGreen (green), β -tubulin-III stained with Alexa Fluor 555 (orange), synaptophysin stained with CF™ 633 (red), and nuclei stained with DAPI (blue).

The introduced technology and platform for biomaterial engineering and biofabrication can print large, predesigned Alg scaffolds that are not only suitable for neural tissue regeneration, but could also be useful for other tissue regeneration applications (see [Outstanding questions](#)). These regenerated tissues could be used for high-throughput drug screening in medicine development or even applied directly in clinical surgeries to address the donor tissue shortage crisis. Additionally, the 3D active tissue model obtained in this study can serve as an *in vitro* model to study efficient computation within the brain and support the development of next-generation ‘computers in a dish’.

STAR★METHODS

Detailed methods are provided in the online version of this paper and include the following:

- KEY RESOURCES TABLE
- METHOD DETAILS
 - Ink preparation and 3D printing
 - Primary cortical neuron isolation and culture
 - Scanning electron microscopy
 - Cell viability evaluation
 - Proliferation and metabolic activity
 - Calcium imaging
 - Immunostaining
- QUANTIFICATION AND STATISTICAL ANALYSIS

RESOURCE AVAILABILITY

Lead contact

Further information and requests for resources and reagents should be directed to and will be fulfilled by the lead contact, Jianfeng Li (jianfeli@mpi-halle.mpg.de).

Materials availability

This study did not generate new unique reagents.

Data and code availability

- All the relevant data are included in the article and the supplementary files.
- This article does not report original code.
- Any additional information will be made available upon reasonable request from the lead contact.

Author contributions

J.L., W.D.S., and J.K.S.P. conceived the study and designed the experiments. B.H., M.B., and H.C. prepared and provided mouse primary neurons. A.R., R.A., and F.S. synthesized and provided t-ZnO microparticles. J.L. performed the 3D printing experiments. J.L., C.W., and T.G. conducted cell experiments and analyzed the results. All authors contributed to the paper and approved the submitted version.

Acknowledgments

The authors are grateful for financial support from the Max Planck Society.

Declaration of interests

The authors declare no competing interests.

Supplemental information

Supplemental information to this article can be found online at <https://doi.org/10.1016/j.tibtech.2024.10.013>.

References

- Langhans, S.A. (2018) Three-dimensional in vitro cell culture models in drug discovery and drug repositioning. *Front. Pharmacol.* 9, 6
- Knowlton, S. *et al.* (2018) Bioprinting for neural tissue engineering. *Trends Neurosci.* 41, 31–46
- Booth, D. *et al.* (2024) Advances in 3D bioprinting for urethral tissue reconstruction. *Trends Biotechnol.* 42, 544–559
- Lorson, T. *et al.* (2020) Sterilization methods and their influence on physicochemical properties and bioprinting of alginate as a bioink component. *ACS Omega* 5, 6481–6486
- Emmermacher, J. *et al.* (2020) Engineering considerations on extrusion-based bioprinting: interactions of material behavior, mechanical forces and cells in the printing needle. *Biofabrication* 12, 025022
- Li, J. *et al.* (2020) 3D printing of cytocompatible graphene/alginate scaffolds for mimetic tissue constructs. *Front. Bioeng. Biotechnol.* 8, 824
- Shuai, C. *et al.* (2018) A graphene oxide-Ag co-dispersing nanosystem: dual synergistic effects on antibacterial activities and mechanical properties of polymer scaffolds. *Chem. Eng. J.* 347, 322–333
- Feng, P. *et al.* (2018) A multimaterial scaffold with tunable properties: toward bone tissue repair. *Adv. Sci.* 5, 1700817
- Shuai, C. *et al.* (2021) Accelerated degradation of HAP/PLLA bone scaffold by PGA blending facilitates bioactivity and osteoconductivity. *Bioact. Mater.* 6, 490–502
- Shuai, C. *et al.* (2024) Oxygen vacancy boosting Fenton reaction in bone scaffold towards fighting bacterial infection. *Int. J. Extreme Manuf.* 6, 015101
- Bose, S. *et al.* (2012) Recent advances in bone tissue engineering scaffolds. *Trends Biotechnol.* 30, 546–554
- Smidsrød, O. and Skjåk-Braek, G. (1990) Alginate as immobilization matrix for cells. *Trends Biotechnol.* 8, 71–78
- Moxon, S.R. *et al.* (2019) Blended alginate/collagen hydrogels promote neurogenesis and neuronal maturation. *Mater. Sci. Eng. C* 104, 109904
- Willems, C. *et al.* (2024) Functionalized gelatin/polysaccharide hydrogels for encapsulation of hepatocytes. *Gels* 10, 231
- Hautmann, A. *et al.* (2022) Free-standing multilayer films as growth factor reservoirs for future wound dressing applications. *Biomater. Adv.* 142, 213166
- Li, J. *et al.* (2019) Smart graphene-cellulose paper for 2D or 3D “origami-inspired” human stem cell support and differentiation. *Colloids Surf. B: Biointerfaces* 176, 87–95
- Vazin, T. and Schaffer, D.V. (2010) Engineering strategies to emulate the stem cell niche. *Trends Biotechnol.* 28, 117–124
- Andersen, T. *et al.* (2013) In situ gelation for cell immobilization and culture in alginate foam scaffolds. *Tissue Eng. A* 20, 600–610
- Neves, M.I. *et al.* (2020) Modulating alginate hydrogels for improved biological performance as cellular 3D microenvironments. *Front. Bioeng. Biotechnol.* 8, 665
- Naghieh, S. *et al.* (2019) Indirect 3D bioprinting and characterization of alginate scaffolds for potential nerve tissue engineering applications. *J. Mech. Behav. Biomed. Mater.* 93, 183–193
- Li, J. *et al.* (2022) Development of 3D printable graphene oxide based bio-ink for cell support and tissue engineering. *Front. Bioeng. Biotechnol.* 10, 994776
- Li, J. *et al.* (2023) 3D printed neural tissues with in situ optical dopamine sensors. *Biosens. Bioelectron.* 222, 114942
- Boularaoui, S. *et al.* (2020) An overview of extrusion-based bioprinting with a focus on induced shear stress and its effect on cell viability. *Bioprinting* 20, e00093
- Hutmacher, D.W. (2000) Scaffolds in tissue engineering bone and cartilage. *Biomaterials* 21, 2529–2543
- Luo, Y. *et al.* (2022) 3D printed hydrogel scaffolds with macro pores and interconnected microchannel networks for tissue engineering vascularization. *Chem. Eng. J.* 430, 132926
- Zhang, X. *et al.* (2023) 3D printed hydrogel/bioceramics core/shell scaffold with NIR-II triggered drug release for chemo-photothermal therapy of bone tumors and enhanced bone repair. *Chem. Eng. J.* 461, 141855
- Majhy, B. *et al.* (2021) Effect of surface energy and roughness on cell adhesion and growth – facile surface modification for enhanced cell culture. *RSC Adv.* 11, 15467–15476
- Hashimoto, T. *et al.* (2005) Peripheral nerve regeneration using non-tubular alginate gel crosslinked with covalent bonds. *J. Mater. Sci. Mater. Med.* 16, 503–509
- Owen, R. *et al.* (2020) Combined porogen leaching and emulsion templating to produce bone tissue engineering scaffolds. *Int. J. Bioprint* 6, 265
- Fuxiang, S. *et al.* (2022) 3D printing calcium alginate adsorbents for highly efficient recovery of U(VI) in acidic conditions. *J. Hazard. Mater.* 440, 129774
- Afjoul, H. *et al.* (2020) Freeze-gelled alginate/gelatin scaffolds for wound healing applications: an in vitro, in vivo study. *Mater. Sci. Eng. C* 113, 110957
- Coluccino, L. *et al.* (2016) Bioactive TGF- β 1/HA alginate-based scaffolds for osteochondral tissue repair: design, realization and multilevel characterization. *J. Appl. Biomater. Funct. Mater.* 14, e42–e52
- Kim, H. *et al.* (2021) Biomaterial-directed cell behavior for tissue engineering. *Curr. Opin. Biomed. Eng.* 17, 100260
- Schulz, A. *et al.* (2018) Tyramine-conjugated alginate hydrogels as a platform for bioactive scaffolds: tyramine-conjugated alginate hydrogels. *J. Biomed. Mater. Res. A* 107, 114–121
- Rowley, J.A. *et al.* (1999) Alginate hydrogels as synthetic extracellular matrix materials. *Biomaterials* 20, 45–53
- Roberge, C.L. *et al.* (2023) Viscoelastic properties of bioprinted alginate microbeads compared to their bulk hydrogel analogs. *J. Biomech. Eng.* 145, 031002
- Banerjee, A. *et al.* (2009) The influence of hydrogel modulus on the proliferation and differentiation of encapsulated neural stem cells. *Biomaterials* 30, 4695–4699
- He, Z. and Yu, Q. (2018) Identification and characterization of functional modules reflecting transcriptome transition during human neuron maturation. *BMC Genomics* 19, 262
- Gleichmann, M. and Mattson, M.P. (2011) Neuronal calcium homeostasis and dysregulation. *Antioxid. Redox Signal.* 14, 1261–1273
- Pchitskaya, E. and Bezprozvanny, I. (2020) Dendritic spines shape analysis—classification or clusterization? *Perspective* 12, 31
- Palazzolo, G. *et al.* (2015) Ultrasoft alginate hydrogels support long-term three-dimensional functional neuronal networks. *Tissue Eng. Part A* 21, 2177–2185
- Hosseinian, M.A. *et al.* (2015) Comparison of a distal end-to-side neurorrhaphy with a proximal–distal end-to-side neurorrhaphy: in a rat model. *Eur. J. Orthop. Surg. Traumatol.* 25, 1261–1264
- Schindelin, J. *et al.* (2012) Fiji: an open-source platform for biological-image analysis. *Nat. Methods* 9, 676–682
- Mishra, Y.K. *et al.* (2013) Fabrication of macroscopically flexible and highly porous 3D semiconductor networks from interpenetrating nanostructures by a simple flame transport approach. *Part. Part. Syst. Charact.* 30, 775–783
- Tomassoni-Ardori, F. *et al.* (2020) Generation of functional mouse hippocampal neurons. *Bio Protoc.* 10, e3702

STAR★METHODS

KEY RESOURCES TABLE

Reagent or resource	Source	Identifier
Antibodies		
Primary mouse anti- β -tubulin III antibody	Sigma-Aldrich	Cat# T8578
Anti-synaptophysin antibody produced in rabbit	Sigma-Aldrich	Cat# SAB4502906
CF™ 633 conjugated secondary donkey anti-rabbit IgG antibody	Sigma-Aldrich	Cat# SAB4600132
Alexa Fluor™ 555 conjugated secondary goat anti-mouse IgG antibody	Biolegend	Cat# 405324
Biological samples		
Primary mouse cortical neurons	Fraunhofer Institute for Cell Therapy and Immunology	Mouse strain (C57BL6/J)
Chemicals, peptides, and recombinant proteins		
Sodium alginate	Sigma-Aldrich	Cat# A2033
Pluronic F-127	Sigma-Aldrich	Cat# P2443
Neurobasal™ Plus Medium	Gibco	Cat# A3582901
B-27™ Plus Supplement (50×)	Gibco	Cat# A3582801
GlutaMAX™ Supplement	Gibco	Cat# 35050061
Critical commercial assays		
Calcein-AM	Sigma-Aldrich	Cat# 206700
Propidium iodide solution	Sigma-Aldrich	Cat# P4864
Hoechst 33342	Miltenyi Biotec	Cat# 130-111-569
PrestoBlue™ cell viability reagent	Invitrogen	Cat# A13262
Calbryte™ 520 AM	AAT Bioquest	Cat# 20650
AlexaFluor™ 488 phalloidin	Invitrogen	Cat# R37110
4',6-diamidino-2-phenylindole	Sigma-Aldrich	Cat# D9542
Deposited data		
Raw data	This paper	doi: 10.17617/3.QRIXLN
Software and algorithms		
ImageJ/Fiji	Schindelin, J. <i>et al.</i> [43]	https://fiji.sc/
Origin 2022b	OriginLab	www.originlab.com/2022b

METHOD DETAILS

Ink preparation and 3D printing

Alg with an average molecular weight (M_n) of 80 000–120 000 from brown algae and Plu with an M_n of 12 600 were purchased from Sigma-Aldrich (Germany).

For 2%/30% (w/w) Alg/Plu ink preparation, 200 mg Alg and 3 000 mg Plu were mixed mechanically with 10.000 g deionized water (DI water) at 4°C for 12 h. Using the prepared 2%/30% (w/w) Alg/Plu ink, 2%/30%/5% (w/w) Alg/Plu/t-ZnO ink was prepared by adding 500 mg t-ZnO into the solution and mixed mechanically at 4°C for another 12 h. Plu was used to modulate the ink's rheological properties, thereby providing it with a higher storage modulus compared to the loss modulus during the printing process, which has been extensively tested and reported in our previous paper [22].

The as-prepared inks were loaded into a 3D printing syringe barrel (Nordson EFD, USA) and centrifuged to de-bubble at 1000 xg for 10 min at 4°C (Fisherbrand Centrifuge, Germany). After centrifugation, t-ZnO microparticles in the ink settled at the bottom part of the

3D printing syringe barrel and were then used directly for scaffold 3D printing (Figure S1 in the supplemental information online). 3D printing was performed using an extrusion-based 3D printer (RegenHU, Switzerland) with a G20 needle (Nordson EFD, USA) fitted in a syringe barrel at room temperature (RT, 21°C). An ink feeding speed of 6 mm/s was used, with the corresponding applied air pressure for each ink (2%/30% (w/w) Alg/Plu ink: 130 kPa; 2%/30%/5% (w/w) Alg/Plu/t-ZnO ink: 170 kPa), followed by 10 min of crosslinking in a 2% (w/v) calcium chloride (CaCl₂; Sigma-Aldrich, Germany) solution at RT. Thereafter, 37% HCl (Fisher Chemical, Germany) was used to remove the t-ZnO component from the crosslinked scaffolds for 3 min, and the scaffolds were reinforced in 2% (w/v) CaCl₂ for another 5 min. The obtained microstructured scaffolds were immersed and washed with copious amounts of DI water to remove the acid residues from the previous step and Plu component in the structure. Before being seeded with cells, the 3D printed scaffolds underwent a sterilization process by immersing in 70% (v/v) ethanol solution for 20 min, followed by desiccation in a biosafety cabinet. A subsequent sterilization procedure was carried out under UV irradiation for 1 h. The sterilized scaffolds were immersed in culture medium overnight in a cell culture incubator (37°C with humidified 5% CO₂; Binder, Germany) before cell seeding. The t-ZnO microparticles used here were synthesized via a previously reported flame transport method [44] with an average arm length of 48.1 μm (*n* = 100), spanning from 13.2 to 116.0 μm [22]. Briefly, t-ZnO microparticles were formed in a furnace (900°C for 20 min) from a mixture of zinc dust (Sigma-Aldrich, Germany) and Mowital B60H (Kuraray Europe, Germany) with a ratio of 1:2. The porosity introduced by the incorporation of t-ZnO microparticles into the microstructured scaffold is defined as:

$$\Phi = \frac{V_{t-znO}}{V_{all}} \quad [1]$$

where Φ is the porosity, V_{t-znO} is the volume of incorporated t-ZnO microparticles in the ink and V_{all} is the overall volume of the ink.

Primary cortical neuron isolation and culture

Primary mouse cortical neurons were isolated from the cortices of mouse (strain C57BL6/J) embryos (E17) as reported previously [45]. The primary cortical cell culture medium comprised Neurobasal™ Plus Medium (Gibco, USA) supplemented with 2% (v/v) B27™ Plus Supplement (Gibco, USA), 1% (v/v) GlutaMAX™ Supplement (Gibco, USA), and 1% (v/v) penicillin-streptomycin (10 000 U/ml; Gibco, USA). The initial cell seeding density for the 3D scaffolds was 0.8×10^5 cells/cm². Cells were cultured in a cell culture incubator, and one-third of the culture medium was changed every three days.

Scanning electron microscopy

For morphology study of 3D printed scaffolds without cells, samples were imaged using a Hitachi TM4000Plus scanning electron microscope (SEM) (Hitachi, Japan) equipped with an ultracool stage at -30°C (Deben, UK). For scaffolds with cells, samples were pretreated by immersing and fixing in 4% paraformaldehyde solution (PFA; ThermoFisher Scientific, Germany) for 30 min. After washing three times with a 2% (w/v) CaCl₂ solution, the samples were imaged using an SEM equipped with an ultracool stage at -30°C. Cross-sectional imaging was performed by fracturing samples using a surgical scalpel.

Cell viability evaluation

For cell viability assessment, staining was performed using 8 μM Calcein AM (CA; Sigma-Aldrich, Germany) for live cell staining, 2 μM propidium iodide (PI; Sigma-Aldrich, Germany) for dead cell staining, and 20 μM Hoechst 33342 (HO; Miltenyi Biotec, Germany) for visualization of nuclei. Briefly, cell-containing structures were incubated with CA for 15 min in a cell culture incubator, followed by addition of PI and HO to the staining medium for another 15 min of incubation. After washing the stained structures with fresh medium, a confocal microscope (Zeiss LSM 900, Germany) was used for imaging.

Proliferation and metabolic activity

The proliferation and metabolic activity of neurons on different 3D scaffolds were assessed using PrestoBlue™ cell viability reagent (ThermoFisher Scientific, Germany) according to the manufacturer's instructions. Briefly, cell-seeded scaffolds were incubated with 500 μl 10% (v/v) reagent culture medium solution for 30 min in an incubator on Days 1 and 7. Subsequently, the supernatant was transferred to a 96-well plate for fluorescence intensity measurement using a microplate reader (excitation/emission: 544/590; POLARstar Omega, Germany). The fluorescence value of the cell-seeded P-Alg scaffolds on Day 1 was set to 100, and the proliferation and metabolic activity on the other samples on Days 1 and 7 were calculated relative to this baseline.

Calcium imaging

Neuronal activity was assessed by staining the neurons with 5 μM Calbryte 520 AM (AAT Bioquest, USA) and 0.04% Plu for 30 min in a cell culture incubator. Plu was used to enhance the cell loading and staining performance of the Calbryte 520 AM. After washing the stained structures with fresh medium, a confocal microscope (Zeiss LSM 900, Germany) with a mounted cell culture incubator (XLmulti S2 DARK, Germany) was used for imaging. ImageJ/Fiji software was used for the analysis of neuronal activity [43].

Immunostaining

Phosphate-buffered saline (PBS; diluted from 10 \times PBS pH 7.4, ThermoFisher Scientific, Germany) and 4% PFA solution were supplemented with 5 mM CaCl_2 to prevent the dissolution of the crosslinked Alg structure. The cell-seeded scaffolds were removed from the culture medium and washed three times with PBS. Subsequently, the cells were fixed with 4% PFA for 30 min at RT. After rinsing three times with PBS, the cells were permeabilized and blocked with 0.3% (v/v) TritonX-100 (Calbiochem, Germany) and 10% (v/v) horse serum (HS; MP Biomedicals, Germany) in PBS for 2 h at RT. Subsequently, the scaffold was incubated overnight at 4 $^{\circ}\text{C}$ with anti- β -tubulin III antibody (1:100; Sigma-Aldrich, Germany) and anti-synaptophysin antibody (1:100; Sigma-Aldrich, Germany) in a 10% (v/v) HS PBS solution. The scaffold was then rinsed three times with PBS and incubated with Alexa FluorTM 555 conjugated secondary goat anti-mouse IgG antibody (1:100; Biolegend, Germany) and CFTM 633 conjugated secondary donkey anti-rat IgG antibody (1:100; Sigma-Aldrich, Germany) for 2 h at RT, followed by incubation with AlexaFluorTM 488 phalloidin (2 drops/ml; ThermoFisher Scientific, Germany) and 4',6-diamidino-2-phenylindole (DAPI, 2 $\mu\text{g}/\text{ml}$; Sigma-Aldrich, Germany) for 1 h at RT. Finally, the scaffold was washed with PBS for three times. Images were acquired using a Zeiss LSM 900 confocal microscope.

QUANTIFICATION AND STATISTICAL ANALYSIS

The proliferation test measurements were conducted in quintuplicate, and the data are presented as the mean \pm standard deviation. Data plotting and statistical analyses were performed using Origin 2022b (OriginLab, USA). Since the Brown-Forsythe test for data variance homogeneity was not satisfied ($P < 0.05$), a significance level of 0.01 was employed for the two-way ANOVA (Bonferroni post hoc test).